THE EFFECT GRINDING AND ANNEALING TEMPERATURE ON MICROSTRUCTURE AND MAGNETIC PROPERTIES OF THE PRESSED POWDER MIXTURE OF 20.0 WT% Fe AND 80.0 WT% $BaTiO_3$

M. SPASOJEVIĆ SAVKOVIĆ[1], M. LUKOVIĆ[2,*], A. MARIČIĆ[2], M. SPASOJEVIĆ[2]

[1] University of Belgrade, Innovative Centre of the Faculty of Chemistry, Studentski trg 12–16 Belgrade, Serbia
[*] *Corresponding author*: milentije.lukovic@ftn.kg.ac.rs
[2] University of Kragujevac, Faculty of Technical Sciences, Joint Laboratory for Advanced Materials of SASA, Section for Amorphous Systems, Svetog Save 65 Čačak, Serbia

Received April 16, 2025

Abstract. The mixture of 20.0 wt% Fe and 80.0 wt% $BaTiO_3$ powders was found to consist of a $BaTiO_3$ matrix and composite particles comprising Fe cores and $BaTiO_3$ shells. During the grinding of this mixture, several processes occur, such as pulverization of the particles of both powders; changes in the size, morphology and composition of aggregates, crushing of crystal grains, increase in the density of chaotically distributed dislocations; growth of internal microstrains; rise in the residual stress; decrease in the amount of crystalline and increase in the amount of amorphous phases, as well as oxidation of Fe into its oxides FeO, Fe_3O_4 and Fe_2O_3. These changes in chemical composition, morphology and microstructure substantially affect the magnetization of the pressed powder mixture. With increasing the grinding time from 0 to 90 min, the increase in magnetization is dominantly affected by crushing of Fe crystal grains. The decrease in magnetization during grinding from 90 to 120 min is caused by the decrease in the amount of metallic Fe by oxidation to FeO and increase in both the density of chaotically distributed dislocations and internal microstrains. Formation of Fe_3O_4 and Fe_2O_3 oxides has a prevailing effect on the increase in magnetization when grinding for longer than 130 min. Chemical and microstructural changes in the mixture of powders of 20.0 wt% Fe and 80.0 wt% $BaTiO_3$ during heating affect the magnetization of cooled samples at 22°C. The powder is thermally stable up to 330°C. The magnetization of samples cooled to 22°C declines with increasing annealing temperature above 330°C. This decrease is caused by both the oxidation of Fe to FeO and formation of larger crystalline grains of Fe. The magnetization of samples heated up to 250°C remains unchanged. At higher temperatures, with increasing the temperature of the sample, its magnetization declines as a result of the transition of directed domains to a chaotic state caused by the effect of thermal energy, formation of larger crystal grains and oxidation of Fe into FeO.

Key words: grinding, pressing, magnetic, $BaTiO_3$ microstructure.

DOI: https://doi.org/10.59277/RomJPhys.2025.70.615

1. INTRODUCTION

Multiferroic materials are research focus of many scientists as their dual polarization, electrical and magnetic, may allow for the application in different

microelectronics devices, such as microwave phase shifters, magnetically controlled electro-optic devices and broadband magnetic field sensors [1–6]. To achieve both magnetism and ferroelectricity in a single-phase material is quite complicate. Therefore, this type of material is very rare and hard to produce. The improved magnetic and electric properties have been accomplished by preparing two-phases systems of multiferroic composite ceramics [7, 16]. Coupling between the ferroelectric and ferromagnetic phase in these composites allows for altering their electric polarization by magnetic field and also modification of magnetic properties by changing the electric field [8].

Among all ferroelectrics, the most commonly studied and applied is $BaTiO_3$ [10–12, 14–28]. This ferroelectric ceramic has been extensively used in piezoelectric devices, such as underwater transduces and multilayer capacitors. However, successful implementation of this material demands fulfilment of certain criteria: high dielectric constants and good resistivity properties in small volumes. The achievement of these requirements has been accomplished by modifying $BaTiO_3$ dielectric with other titanates.

Multiferroics materials are prepared by combining ferroelectrics and ferromagnetics. Multiferroic films have been obtained from ferroelectric $BaTiO_3$ and ferromagnetic pure metals and their oxides [6, 10, 13, 16, 17]. Many research groups focused on development of multiferroic composites whose ferromagnetic comprises two oxide phases with desired properties. However, metals prevailed in use since they have strong ferromagnetic properties even at room temperature, typically much stronger than those of their oxide counterparts [11–15, 20, 22, 23].

This research is based on use $BaTiO_3$ as a matrix and Fe as a magnetic secondary phase. Our previous study has shown that Fe particles embedded in the $BaTiO_3$ matrix are strong ferromagnets [14]. In the Fe-$BaTiO_3$ nanocomposite strong coupling between the Fe and $BaTiO_3$ particles is achieved by a large interface strain provided by the composite structure. The strength of this ferromagnetic system is determined by the properties of Fe particles: the mean particle size, particle morphology and density. Various preparation methods of these materials are reported in literature and affect the microstructure, morphology, electrical and magnetic properties of Fe-$BaTiO_3$ nanocomposites [6–12, 10–28]. The ball milling has been lately reported as a preparation method which allows for production of different nanostructures and various magnetic materials. The grinding time was found to be a very important parameter, which affected not only morphology and microstructure, but also magnetic and electric properties of powders. Thus, the magnetic and electrical properties can be tuned by appropriate selection of grinding time [11, 14–16, 23, 25].

In this paper the effects of the grinding time of a powder mixture of 20.0 wt% Fe and 80.0 wt% $BaTiO_2$ on the morphology, microstructure and magnetic properties of the obtained samples was examined. Additionally, it was aimed to investigate an influence of annealing of the ground mixture in the temperature range from 22°C to

620°C on the above-mentioned characteristics. According to the gathered experimental results, the optimal conditions for the preparation of samples with desired properties were defined.

2. EXPERIMENTAL

First, a suspension of $BaTiO_3$ (Aldrich, St. Louis, MO, p.a. 99 wt%) in 2-propanol was ground for 20 min in a planetary ball mill (Retsch PM 400) in air. Then, a suspension of a powder mixture of 20.0 wt% Fe (Aldrich, St. Louis, MO, p.a. 99.99) and 80.0 wt% $BaTiO_3$ was ground for 20 min to 220 min. Disc-shaped samples (8.0 mm in diameter and 1.5 mm in thickness) were prepared by pressing the powder mixture under pressure of 500 MPa. The X-ray images were obtained using Bruker DM X-ray diffraction instrument in Bragg-Brentano geometry with a grazing incidence angle of 0.5° using $CuK_{\alpha,1}$ ($\lambda_{K\alpha,1}$ = 0.15406 nm) radiation. Diffraction data were acquired over the scattering angle 2θ from 10° to 90° with step of 0.05°. The morphology, particle and aggregate size were analyzed using a Scanning Electron Microscope (SEM, JSM-6390 LV JEOL, 30 kV) coupled with EDS and by a Leica Q500 MC automatic device for the microstructural analysis. Magnetic measurements were performed by a modified Faraday method based on the effect of an inhomogeneous magnetic field of the sample. Magnetic force measurements were carried out with sensitivity of 10^{-7} N under argon atmosphere.

3. RESULTS AND DISCUSSION

The phase structure of samples prepared by thorough mixing of either unground or ground mixture of 20.0 wt% Fe and 80.0 wt% $BaTiO_3$ powders was determined by XRD-analysis. Four X-ray images were recorded for each sample, wherein no substantial differences between radiographs of the same sample were detected. In the X-ray image of the unground sample well-defined peaks of $BaTiO_3$ and barely noticeable peaks of different Fe planes were observed (Fig. 1a). Our previous study has demonstrated effective adsorption of small ground particles of $BaTiO_3$ (less than 5 μm large) with an extensive number of surface defects on the surface of Fe particles [14]. This indicated the structure of the mixture of 20 wt% Fe and 80 wt% $BaTiO_3$, which consisted of a $BaTiO_3$ matrix with embedded composite particles composed from Fe core and $BaTiO_3$ shell [14].

The thickness of the $BaTiO_3$ shell affects the effectiveness of X-ray penetration to the Fe core and thus, the intensity of Fe-peaks in the XRD images. The peaks corresponding to Fe are hardly observed in Fig. 1 since the $BaTiO_3$ particles absorbed on the surface of Fe particles obscure the passage of X-rays. The effect of the increase in grinding time is shown in roentgenograms of Fig. 1 through: a) the proportional decrease in the intensity of all $BaTiO_3$ peaks, b) increase in the width of their half-

height and c) decline of integral of their intensities. Thus, the above experimental results indicate that the increase in grinding time results in a) unchanged texture of $BaTiO_3$ crystals, b) the increase in the density of chaotically distributed dislocations and internal microstrains and c) the decline in the quantity of the crystalline $BaTiO_3$ phase (Fig. 2) [11, 14–16, 29–33].

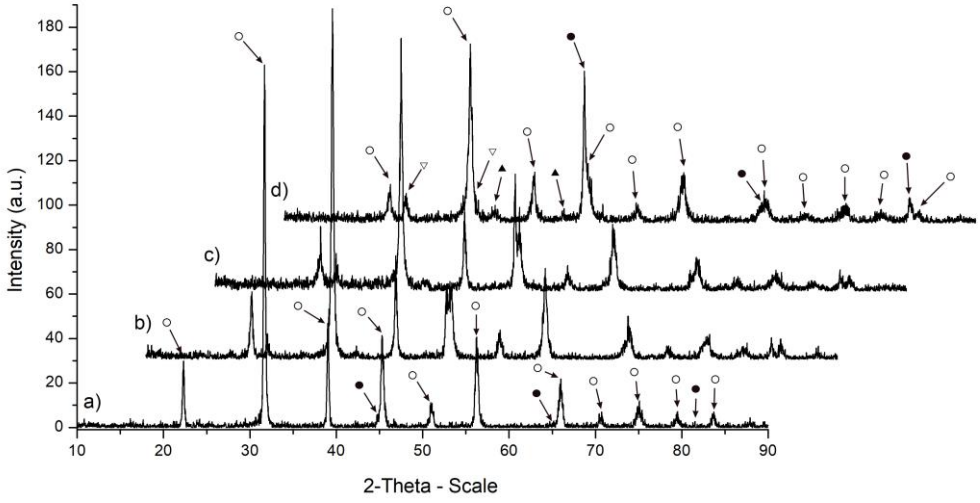

Fig. 1 – XRD patterns of the samples ground for: a) 0 min, b) 120 min, c) 180 min, d) 270 min; ○ – $BaTiO_3$; ● – α-Fe; ▲ – Fe_3O_4 and s – Fe_2O_3.

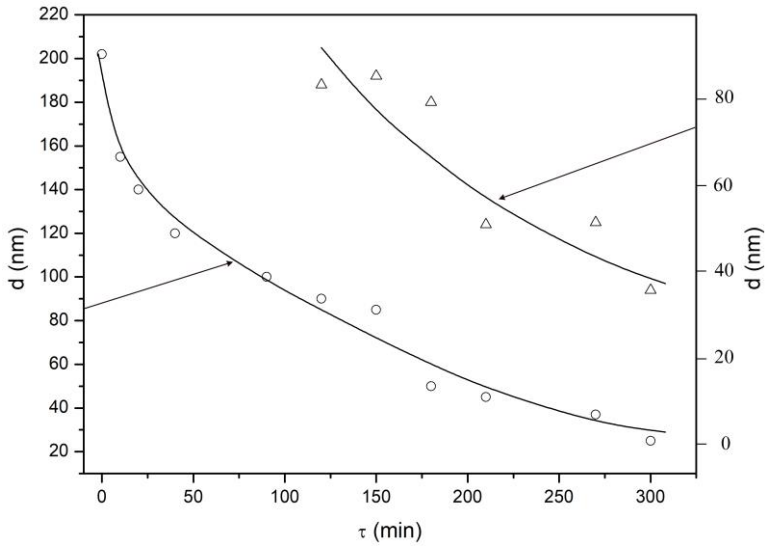

Fig. 2 – The mean crystals size as a function of grinding time: ○ – $BaTiO_3$ and △ – Fe.

During grinding, the particles and crystal grains of Fe and $BaTiO_3$ are crushed by the effect of mechanical force (Fig. 2). This results in appearance of new dislocations in the powders and simultaneous growth of internal microstrains. Since the thermal energy, formed by transformation of the mechanical energy, induces the greatest raise of temperature in the surface layer of particles, the appearance of new dislocations and the internal microstrains growth are particularly conspicuous on the particles surface. These phenomena cause disruption of crystal structure of that layer [11, 14–16]. Thus, the grinding process results in formation of the amorphous phase.

An increase in both the temperature and number of defects in the surface layer of the Fe particles accelerates the oxidation of that layer by atmospheric oxygen, which further results in the Fe/Fe_xO_y particles formation. These new particles are composed of the Fe core and Fe_xO_y oxide shell [11, 14–16]. The presence of Fe_xO_y is confirmed by XRD and EDS spectra, showing an increase in the oxygen content in the powder with increase in grinding time (Fig. 1 and Fig. 3).

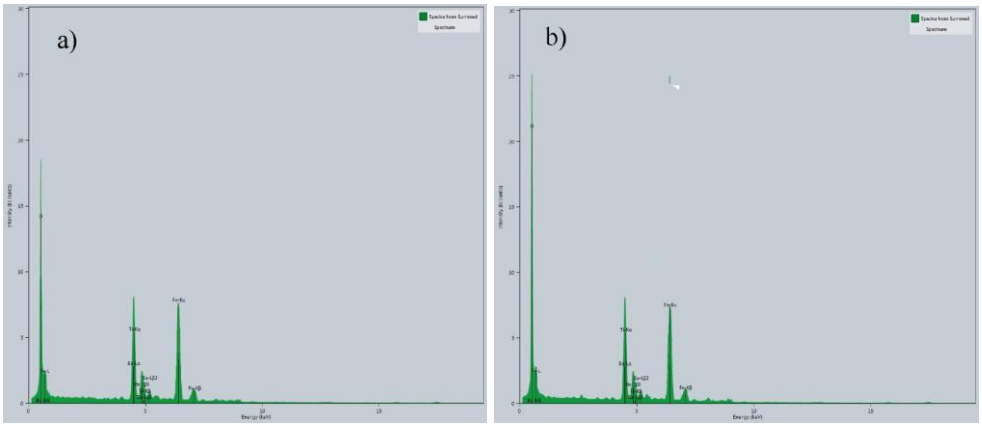

Fig. 3 – EDS spectra of powder ground for: a) 70 min, b) 160 min.

Roentgenograms in Fig. 1 also show an increase in both the intensity and width of the half-height of weakly expressed peaks of Fe with rising grinding time. The grinding results in shredding of the particles of Fe and $BaTiO_3$ causing an increase in their total surfaces. Simultaneously, aggregates of Fe particles, $BaTiO_3$ particles and mixed aggregates of Fe particles and $BaTiO_3$ particles are formed. As shown by the SEM micrographs and chemical mapping of the powders, an increase in the grinding time causes: a) the decline in the mean size of particles and b) increase in the mean size of aggregates, reaching its maximum in 150 min. When increasing the grinding time from 150 min to 240 min the mean size of aggregates declines (Table 1) [14–15].

Table 1

Effect of grinding time on the mean particle size and mean aggregate size of $BaTiO_3$ and Fe/Fe_xO_y

	Mean particle size (nm)		Mean aggregate size (μm)	
Grinding time (min)	$BaTiO_3$	Fe/Fe_xO_y	$BaTiO_3$	Fe/Fe_xO_y
0	3200	15500	/	/
60	370	810	1.6	5.1
90	270	510	1.8	5.9
120	200	310	2.2	6.3
150	170	220	2.6	6.5
180	150	190	2.4	3.1
240	140	140	1.8	1.8

Chemical mapping was used to determine the structure of the initial mixture of powders and powders ground for less than 120 min. These powders are composed of a matrix consisting of particles and aggregates of $BaTiO_3$ wherein the particles of Fe/Fe_xO_y and its aggregates are embedded. However, longer grinding results in formation of the mixed aggregates of $BaTiO_3$ and Fe/Fe_xO_y particles [14]. With increasing grinding time, the content of Fe/Fe_xO_y particles in the initial $BaTiO_3$ aggregates rises as well as the content of $BaTiO_3$ particles in the initial Fe/Fe_xO_y aggregates. Aggregates with an even distribution of $BaTiO_3$ and Fe/Fe_xO_y particles are formed in the powders ground for longer than 200 min. The decline in the mean particle size with increasing grinding time (Table 1) causes formation of a thinner layer of $BaTiO_3$ absorbed on Fe/Fe_xO_y particles. This allows for easier penetration of X-rays to the Fe nuclei and results in the increased intensity of Fe peaks. Therefore, the presented results show the effect of time of grinding of the initial mixture consisting of 20.0 wt% Fe and 80.0 wt% $BaTiO_3$ on the morphology and microstructure of the ground mixture, and thus their magnetic and electrical properties. Magnetic properties of the pressed samples at 500 MPa were examined by determining the dependence of magnetization on grinding time and annealing temperature. The effect of grinding time of the starting powder on magnetization of the pressed samples is shown in Fig. 4.

Figure 4 shows the rise in the magnetization when increasing grinding time up to 90 min. Then the magnetization declines with further grinding and reaches its minimum value in samples ground for 140 min. Subsequently, the magnetization increases when grinding for more than 140 min. The grinding results in changes in the morphology, chemical composition and microstructure of the powder mixture, causing alteration in its magnetization. During powder grinding, several processes occur: a) crushing of crystals and particles, b) increase in the density of chaotically distributed dislocations and internal microstresses, c) formation of the amorphous phases and oxides, d) FeO, e) Fe_3O_4 and f) Fe_2O_3, and g) decrease in the amount of metallic Fe

[11, 14–16, 23]. In the first-time interval from 0 to 90 min, the processes a) and f) result in an increase in magnetization, whereas the processes b), c) and d) cause the magnetization decline [11, 14, 16]. Shredding of iron crystals is a leading effect, resulting in the increased magnetization when the grinding time rises up to 90 min. The powder with finer crystals allows for a) an easier orientation of magnetic domains and b) a greater mobility of domain walls and thus, greater widening of the walls [11, 14, 16, 30, 32, 33]. The decrease in magnetization of the pressed powder within the grinding time interval of 90 to 140 min is a consequence of a lowering in the content of metallic iron, formation of FeO and an increase in both the density of chaotically distributed dislocations and inner microstrains [11, 14]. The formation of Fe_3O_4 and Fe_2O_3 is a dominant effect that determines the magnetization during grinding for longer than 140 min. EDS images corroborate the intensive formation of these oxides when grinding for longer than 130 min. The effect of temperature of the pressed powder on its magnetization and an impact of annealing temperature on the magnetization at 22°C were studied. To this purpose, a pressed sample obtained from powder ground for 90 min was used since grinding for this period of time provides the powder with the highest magnetization at 22°C. The sample was heated at a rate of 15°C min^{-1} to the desired temperature t_{max} and its magnetization was simultaneously determined. Then, it was annealed for 15 min at t_{max} and subsequently cooled to 22°C (the cooling rate was 15°C min^{-1}). This process was repeated three times, wherein each time a different sample was tested. Subsequently, the samples were heated at the same rate to higher temperature. The heating and cooling cycle was performed seven times. Each subsequent cycle involved the sample heating to higher temperature (Fig. 5).

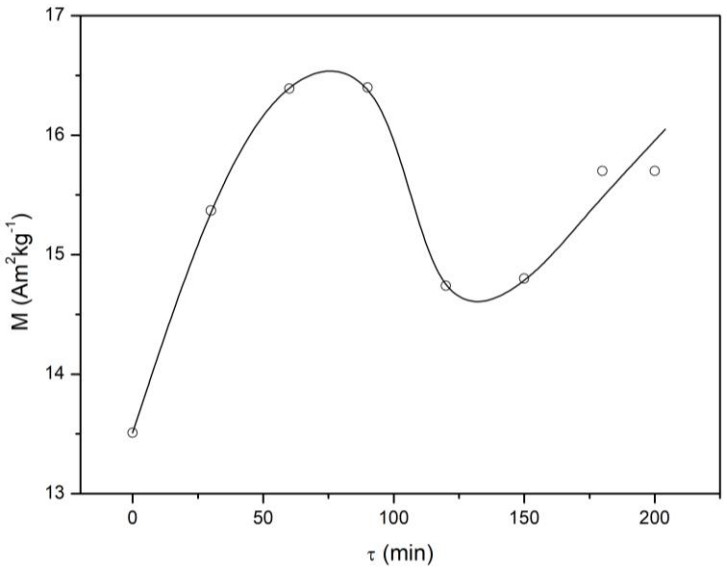

Fig. 4 – Magnetization M of the pressed samples as a function of the grinding time τ at 22°C. The strength of the external magnetic field was 50 kAm^{-1}.

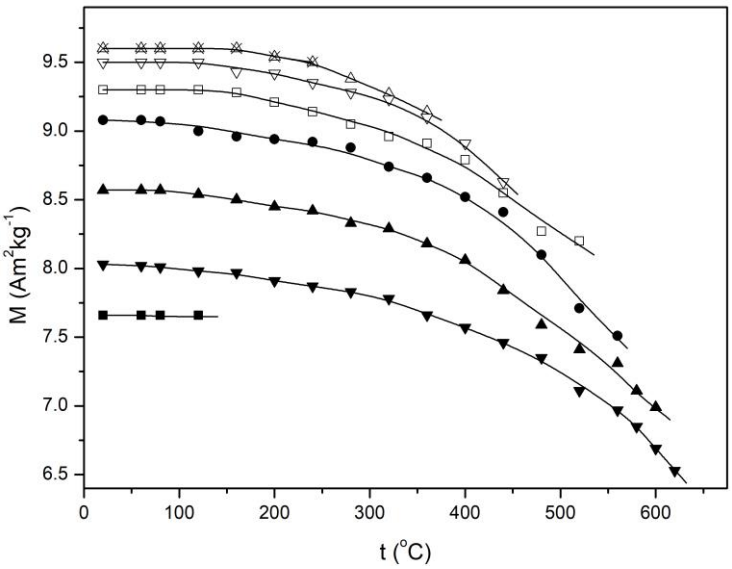

Fig. 5 – Temperature dependence of magnetization M of the pressed powder obtained from the powder ground for 111 min: × – the first heating to 250°C; △ – the second heating to 360°C; ● – the third heating to 450°C; ■ – the forth heating to 450°C, ▲ – the fifth heating to 500°C; □ – the sixth heating to 600°C and ▽ – the seventh heating to 620°C.

Dependence of the magnetization of the pressed sample cooled to 22°C on maximum temperature t_{max} of the previous annealing is presented in Fig. 6.

As seen in Fig. 6 the magnetization of the cooled sample remains consistent after previous annealing at temperatures of up to 330°C, indicating the thermal stability of the sample up to 330°C. In the temperature range of 330 to 500°C, the magnetization of the cooled sample slowly decreases. The X-ray analysis reveals a slight decline in the intensity of Fe peaks and a minor increase in the width of their half-height with the temperature rise in this interval. Also, the iron oxide peaks are invisible in the X-ray roentgenograms, indicating oxidation of Fe crystals mainly into amorphous FeO. In this temperature interval, several processes occur: a) the structural relaxation, b) increase in the size of Fe crystals, c) oxidation of Fe to FeO and d) FeO oxidation to Fe_3O_4 and Fe_2O_3. The processes a) and d) cause an increase in the magnetization of the cooled samples, whereas the processes b) and c) result in the magnetization decline [11, 14, 16, 30, 32, 33]. The processes a) and c) mainly occur in the temperature range of 330 to 500°C, as revealed by the presented experimental results. The effect of process c) prevails over process a) resulting in a magnetization drop.

In the temperature range of 330 to 500°C an increase in temperature causes a slight change in the relaxation rate and an increase in the intensity of Fe oxidation to FeO, inducing an increase in the magnetization rate drop of the cooled

sample. The X-ray image of the cooled samples heated above 500°C shows the Fe peaks of lower intensity and narrower half-height widths. Weak peaks of FeO and barely visible peaks of Fe_3O_4 are also observed in the X-ray roentgenogram. These results indicate the increased oxidation of Fe into its oxides and formation larger crystalline grains of Fe at higher temperatures. Therefore, the heating above 500°C results in a rapid increase in the magnetization drop of the cooled samples.

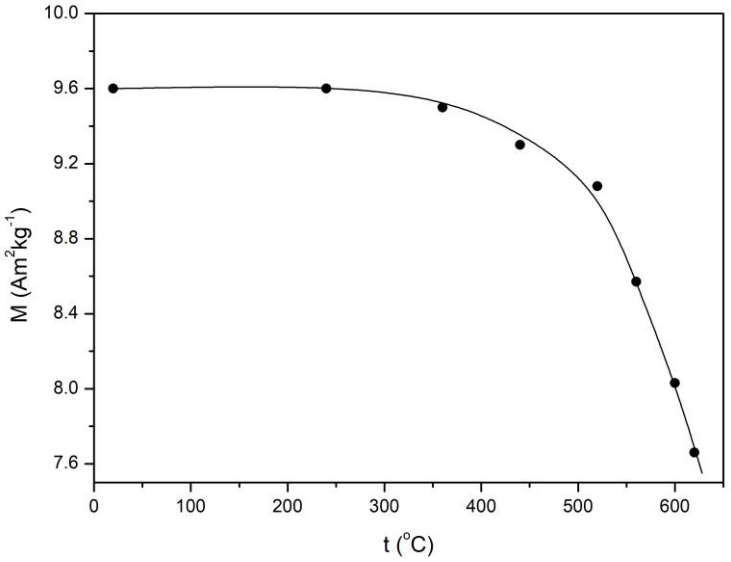

Fig. 6 – Magnetization M of the pressed powder ground for 90 min at 22°C as a function of maximum temperature t_{max} of previous annealing. The strength of an external magnetic field was 50 kAm^{-1}.

Magnetization also depends on the temperature of the sample (Fig. 5). When heating the samples from 22 to 250°C, the magnetization remains consistent since irreversible microstructural changes and chemical reactions do not occur at these temperatures. Also, the thermal energy is insufficient to transform directed magnetic domains into a chaotic state. The decrease in magnetization of sample heated above 250°C results from the transition of directed magnetic domains into a chaotic state caused by the effect of thermal energy, formation of larger crystalline grains and formation of FeO by oxidation of Fe [11, 14, 16, 30, 32, 33]. Thermal energy induces a sharp drop in magnetization when heating above 500°C. At temperatures higher than 330°C, the processes that increase the magnetization are: the decline in the density of chaotically distributed dislocations, internal microstrains and residual stress in Fe crystals and oxidation of FeO into Fe_3O_4 and Fe_2O_3. However, the effect of these processes is substantially less expressed than the effect of the processes that cause a decrease in magnetization (Fig. 5) [11, 14, 16, 30, 32, 33].

The analysis of the obtained results indicates that highest magnetization at 22°C was achieved with the powder 20.0 wt% Fe and 80.0 wt% $BaTiO_3$ ground for 90 min. Also, this sample is magneto-thermally stable in the temperature range from 22 to 330°C.

4. CONCLUSIONS

Thoroughly blended mixture of either unground or ground powders of 20.0 wt% Fe and 80.0 wt% $BaTiO_3$ consists of $BaTiO_3$ matrix and composite particles composed of Fe cores and $BaTiO_3$ shells. During grinding, the several processes occur: a) pulverization of the particles of both powders; b) change in the morphology, size and composition of aggregates of the powder particles; c) crushing of crystal grains; d) increase in the density of chaotically distributed dislocations; e) growth of internal microstrains; f) increase in the residual stress; g) decrease in the amount of crystalline and increase in the amount of the amorphous phases, and h) oxidation of metallic Fe into its oxides: FeO, Fe_3O_4 and Fe_2O_3. With increasing grinding time from 0 to 90 min, the magnetization rises and reaches its maximum for powders ground for 90 min. The dominant effect of the magnetization change in this grinding interval is crushing of the iron crystal grains. The powder with smaller crystals has magnetic domains that are easier to arrange and magnetic walls of higher mobility [11, 14, 16, 30, 32, 33]. The decline in magnetization when grinding the sample from 90 to 140 min is attributed to lowering of the content of metallic iron, formation of FeO and increase in both the density of chaotically distributed dislocations and inner microstrains [11, 16]. The formation of Fe_3O_4 and Fe_2O_3 oxides dominantly affects the magnetization rise after grinding for more than 130 min.

Heating temperature of the pressed powder induces changes in the chemical composition and microstructure, thus affecting the magnetization of the cooled samples at 22°C. When annealing the samples to 330°C, the microstructure and magnetization of samples cooled to 22°C remain unchanged. In the temperature range of 330 to 500°C, the rate of oxidation of Fe to FeO oxide rises with increasing temperature, causing a rapid decline in the magnetization of the cooled sample. Rapid drop in magnetization of the cooled samples after their annealing above 500°C is caused by both substantially more intense oxidation of Fe into FeO and the growth of Fe crystal grains with the temperature increase.

Magnetization of heated samples at temperatures from 22°C to 250°C is similar. When heating the sample above 250°C, with increasing temperature the magnetization of the heated samples decreases due to transition of directed domains into a chaotic state resulting from the effect of thermal energy, formation of larger crystal grains and oxidation of Fe to FeO [11, 14, 16, 30, 32, 33]. A sudden

drop in the magnetization at temperatures above 500°C is caused by the thermal energy.

Acknowledgements. This study was supported by the Ministry of Science, Technological Development and Innovation of the Republic of Serbia, Grant No. 451-03-66/ 2024-03/200132 University of Kragujevac – Faculty of Technical Sciences Čačak and Grant No. 451-03-66/2024-03/200288, University of Belgrade – Innovative Centre of the Faculty of Chemistry.

REFERENCES

1. Aarts, J., Advanced Materials **5**, 221–222 (1993).
2. Scott J. F., Nature Materials **6**, 256–257 (2007).
3. Nan C. W., Bichurin M. I., Dong S., Viehland D., and Srinivasan G., Journal of Applied Physics **103**, 031101 (2008).
4. Wang K. F., Liu J. M., and Ren Z. F., Advances in Physics **58**, 321–448 (2009).
5. Pullar R. C., Progress in Materials Science **57**, 1191–1334 (2012).
6. Gao X., Li L., Jian J., Wang H., Fan M., Huang J., Wang X. and Wang H., ACS Applied Nano Materials **1**, 2509–2514 (2018).
7. Shandilya M. and Verma R., Journal of Magnetism and Magnetic Materials **527**, 167782 (2021).
8. Yamasaki Y., Miyasaka S., Kaneko Y., He J. P., Arima T., and Tokura Y., Physical Review Letters **96**, 207204 (2006).
9. Haque A., Mahbub A. R., Abdullah-Al Mamun M., Reaz M., Ghosh K., Applied Physics A: Materials Science and Processing **125**, 1–9 (2019).
10. Filipović S., Obradović N., Andjelković Lj., Olćan D., Petrović J., Mitrović M., Pavlović V., Jeremić D., Vlahović B., Djordjević A., Science of Sintering **53**, 1–8 (2021).
11. Plazinic M., Spasojevic M., Lukovic M., Maricic A., and Spasojevic M. D., Journal of Optoelectronics and Advanced Materials **23**, 383–396 (2021).
12. Zhang B., Huang J., Rutherford B. X., Lu P., Misra S., Kalaswad M., He Z., Gao X., Sun X., Li L., Wang H., Materials Today Nano **11**, 100083 (2020).
13. Zhang W., Fan M., Li L., Chen A., Su Q., Jia Q., MacManus-Driscoll J. L., Wang H., Applied Physics Letters **107**, 212901 (2015).
14. Kosić O., Luković M., Spasojević-Savković M., Maričić A., Spasojević M., Science of Sintering **56**, 03, 381–383 (2024).
15. Luković M., Spasojević-Savković M., Kosić O., Barudžija T., Lojpur V., Maričić A., Spasojević M., Science of Sintering **57**, 02, 1–18 (2025).
16. Spasojević M., Luković M., Arnaut S., Maričić E., Spasojević M., Materials Chemistry and Physics **283**, 125987 (2022).
17. Shandilya M., Rai R., Sharma K., Thakur D., Integrated Ferroelectrics **185**, 147–154 (2017).
18. Salcedo-Abraira P., Morán E., Villafuerte-Castrejón M. E., Vivar-Ocampo R., Pardo L., Advanced Applied Ceramics **117**, 72–77 (2018).
19. Reaz M., Haque A., Ghosh K., Nanomaterials **10**, 563 (2020).
20. Paunović V., Mitić V., Đorđević M., Marjanović M., Kočić L., Science of Sintering **49**, 129–137 (2017).
21. Ray Mal J., Hing P., Journal of Applied Physics **88**, 1008–1014 (2000).
22. Nakayama H., Katayama-Yoshida H., Japanese Journal of Applied Physics **40**, L1355–L1358 (2001).
23. Živojinović J., Kosanović D., Blagojević V. A., Pavlović V. P., Tadić N., Vlahović B., Pavlović V. B., Science of Sintering **54**, 401–414 (2022).

24. Ranđelović B. M., Ribar S., Mitić V. V., Marković B., Fecht H., Vlahović B., Science of Sintering **54**, 425–438 (2022).
25. Paunović V., Prijić Z., Mitić V. V., Science of Sintering **54**, 81–91 (2022).
26. Reddy V. N., Babu Naidu K. C., Subbarao T., Journal of Ovonic Research **12**, 185–191 (2016).
27. Jin L., Li B., Zhang H., Lin H. Y. G., Wang H., Lin P. T., ACS Applied Materials & Interfaces **9**, 21848–21855 (2017).
28. Rani A., Kolte J., Vadla S. S., Gopalan P., Ceramics International **42**, 8010–8016 (2016).
29. Spasojević M. D., Krstajić N. V., Jakšić M. M., Journal of Molecular Catalysis **40**, 311–326 (1987).
30. Ribić-Zelenović L., Spasojević M., Maričić A., Ristić M. M., Science of Sintering **41**, 175–184 (2009).
31. Ćirović N., Spasojević P., Ribić-Zelenović L., Mašković P., Spasojević M., Science of Sintering **47**, 347–365 (2015).
32. Ćirović N., Spasojević P., Ribić-Zelenović L., Mašković P., Maričić A., Spasojević M., Science of Sintering **48**, 1–16 (2016).
33. Spasojević M., Ćirović N., Ribić-Zelenović L., Spasojević P. and Maričić A., Journal of the Electrochemical Society **161**, D463 (2014).